

# Electronic stopping power of aluminum crystal

I. Campillo, J. M. Pitarke

*Materia Kondentsatuaren Fisika Saila, Zientzi Fakultatea, Euskal Herriko Unibertsitatea,  
644 Posta kutxatila, 48080 Bilbo, Basque Country, Spain*

A.G. Eguiluz

*Department of Physics and Astronomy, The University of Tennessee, Tennessee 37996-1200  
and Solid State Division, Oak Ridge National Laboratory, Oak Ridge, Tennessee 37831-6032*

(October 30, 2018)

## Abstract

Ab initio calculations of the electronic energy loss of ions moving in aluminum crystal are presented, within linear-response theory, from a realistic description of the one-electron band-structure and a full treatment of the dynamical electronic response of valence electrons. For the evaluation of the density-response function we use the random-phase approximation and, also, a time-dependent extension of local-density functional theory. We evaluate both position-dependent and random stopping powers, for a wide range of projectile velocities. Our results indicate that at low velocities band structure effects slightly enhance the stopping power. At velocities just above the threshold velocity for plasmon excitation, the stopping power of the real solid is found to be smaller than that of jellium electrons, corrections being of about 10%. This reduction can be understood from sum rule arguments.

Typeset using REVTeX

## I. INTRODUCTION

The stopping power for charged particles penetrating a solid has been the topic of considerable theoretical and experimental interest, since the beginning of this century<sup>1–4</sup>. The electronic stopping power due to collisions with valence electrons has been evaluated for many years on the basis of a jellium model<sup>5,6</sup> of the target, the electronic states being described by plane waves. However, in a more realistic approach valence electrons move in a periodic potential, electronic states are described by Bloch wave functions, and the spectrum of one-electron excitations splits into the so-called energy bands. The impact of band structure effects on both plasmon dispersion curves<sup>7</sup> and dynamical structure factors<sup>8–10</sup> has been investigated recently, demonstrating the importance of these effects even in the case of free-electron-like metals such as aluminum.

Among the most recent attempts to fully introduce the electronic band structure in the evaluation of the stopping power for low projectile velocities there is, for alkaline metals, a one-band calculation<sup>11</sup>, as well as a calculation based on a linear combination of atomic orbitals<sup>12</sup>. For arbitrary incident velocities the stopping power can be calculated, within linear-response theory, from the knowledge of the dynamical density-response function of the target<sup>13–15</sup>. Approximate semiempirical treatments of this quantity have been made, and stopping powers of silicon<sup>16–19</sup> and gold<sup>20</sup> for channeled ions have been predicted. More recently, the low velocity limit has been investigated, on the basis of a static treatment of the density-response<sup>21</sup>. First-principles treatments of the full dynamical electronic response of various solids have also been performed, and preliminary ab initio evaluations of the stopping power of real solids have been presented<sup>22–24</sup>.

In this paper we investigate, within linear-response theory, the valence electronic energy loss of ions moving through aluminum crystal. Aluminum is well known to be a typical jellium-like metal with a well-defined excitation spectrum, and it represents, therefore, an appropriate benchmark for ab initio evaluations of the electronic stopping power of real solids. First of all, in section II we describe our full treatment of the wave-vector and fre-

quency dependent electronic response of valence electrons, based on a realistic description of the one-electron band structure and first-principles pseudopotential theory. For the evaluation of the density-response function we use the random-phase approximation (RPA)<sup>25</sup> and, also, a time-dependent extension of local-density functional theory (TDLDA)<sup>26</sup>. In section III, we derive explicit expressions for both random and position-dependent stopping powers, from the knowledge of the imaginary part of the projectile self-energy, which is evaluated in the so-called GW approximation<sup>27</sup>. In section IV, numerical calculations of the stopping power of valence electrons in aluminum crystal are presented, for a wide range of projectile velocities, and we compare our results with the stopping power of a homogeneous electron gas with a density equal to that of aluminum. We evaluate, separately, contributions to the energy loss coming from the excitation of single electron-hole pairs and plasmons, and we interpret our results on the basis of the f-sum-rule for the dynamical structure factor. We only consider the electronic response of valence electrons, and the contribution to the electronic stopping power coming from the excitation of core electrons is, therefore, not taken into account. In section V, our conclusions are presented.

## II. DENSITY-RESPONSE FUNCTION

The linear density-response function  $\chi(\mathbf{r}, \mathbf{r}', \omega)$  of an electron system is defined by the equation

$$\rho^{ind}(\mathbf{r}, \omega) = \int d^3\mathbf{r}' \chi(\mathbf{r}, \mathbf{r}', \omega) V^{ext}(\mathbf{r}', \omega), \quad (2.1)$$

where  $\rho^{ind}(\mathbf{r}, \omega)$  is the electron density induced by an external potential  $V^{ext}(\mathbf{r}, \omega)$ .

In a *self-consistent-field* theory, the induced electron density is derived from the response function  $\chi^0(\mathbf{r}, \mathbf{r}', \omega)$  for non-interacting electrons moving in an effective potential  $V_{eff}(\mathbf{r}, \omega)$ , as follows

$$\rho^{ind}(\mathbf{r}, \omega) = \int d^3\mathbf{r}' \chi^0(\mathbf{r}, \mathbf{r}', \omega) [V^{ext}(\mathbf{r}', \omega) + V^{ind}(\mathbf{r}', \omega)], \quad (2.2)$$

where  $V^{ind}(\mathbf{r}, \omega)$  represents the linear change in  $V_{eff}(\mathbf{r}, \omega)$  brought about by the induced electron density itself. Since we consider a time-dependent external field, we are in the more general scenario of time-dependent density functional theory (DFT)<sup>28</sup>, whose theorems<sup>29</sup> generalize those of the usual DFT<sup>30</sup>.

Within time-dependent DFT,  $V^{ind}(\mathbf{r}, \omega)$  consists of the sum of two terms (we use atomic units throughout, i. e.,  $m_e = e = \hbar = 1$ ): The Hartree contribution,

$$V_H^{ind}(\mathbf{r}, \omega) = \int d^3\mathbf{r}' \frac{1}{|\mathbf{r} - \mathbf{r}'|} \rho^{ind}(\mathbf{r}', \omega), \quad (2.3)$$

which accounts for the average (long-range) effects of the Coulomb interaction between the target electrons, and the exchange-correlation (XC) contribution,

$$V_{xc}^{ind}(\mathbf{r}, \omega) = \int d^3\mathbf{r}' \frac{\delta V_{xc}[\rho]}{\delta \rho(\mathbf{r}, \omega)} \rho^{ind}(\mathbf{r}', \omega), \quad (2.4)$$

which accounts for the effects of all many-body short-range correlations not included in the Hartree approximation. Here,  $V_{xc}$  represents the functional derivative of the XC energy functional  $E_{xc}$ :

$$V_{xc}[\rho] = \frac{\delta E_{xc}[\rho]}{\delta \rho(\mathbf{r}, \omega)}. \quad (2.5)$$

Introduction of Eqs. (2.3) and (2.4) into Eq. (2.2) and comparison with Eq. (2.1) result in the following integral equation for the self-consistent-field density-response function:

$$\chi(\mathbf{r}, \mathbf{r}'; \omega) = \chi^0(\mathbf{r}, \mathbf{r}'; \omega) + \int d\mathbf{r}_1 \int d\mathbf{r}_2 \chi^0(\mathbf{r}, \mathbf{r}_1; \omega) V(\mathbf{r}_1, \mathbf{r}_2; \omega) \chi(\mathbf{r}_2, \mathbf{r}'; \omega), \quad (2.6)$$

where

$$V(\mathbf{r}, \mathbf{r}'; \omega) = \frac{1}{|\mathbf{r} - \mathbf{r}'|} + K_{xc}[\rho] \quad (2.7)$$

and

$$K_{xc}[\rho] = \frac{\delta^2 E_{xc}[\rho]}{\delta \rho(\mathbf{r}, \omega) \delta \rho(\mathbf{r}', \omega)}. \quad (2.8)$$

In the time-dependent Hartree or random-phase approximation,  $V_{eff}(\mathbf{r})$  consists only of the average electrostatic interaction between the electrons, the induced potential is then

given by the Hartree term exclusively, and  $K_{xc}(\mathbf{r}, \mathbf{r}')$  in Eq. (2.7) is taken to be zero. In the TDLDA, the kernel  $K_{xc}(\mathbf{r}, \mathbf{r}')$  entering Eq. (2.7) is replaced by

$$K_{xc}(\mathbf{r}, \mathbf{r}')^{LDA} = \delta(\mathbf{r} - \mathbf{r}') \left[ \frac{dV_{xc}(\rho)}{d\rho} \right]_{\rho=\rho_0(\mathbf{r})}, \quad (2.9)$$

where  $V_{xc}(\rho)$  is the derivative of the XC energy of a homogeneous electron gas of density  $\rho$ , which we compute with use of the Perdew and Zunger parametrization<sup>31</sup>. This so-called TDLDA represents an adiabatic extension (a zero frequency  $K_{xc}$  is used) to finite frequencies of the local density approximation (LDA) for XC.

For periodic crystals we introduce a Fourier expansion of the density-response function,

$$\chi(\mathbf{r}, \mathbf{r}', \omega) = \frac{1}{\Omega} \sum_{\mathbf{q}} \sum_{\mathbf{G}, \mathbf{G}'}^{BZ} e^{i(\mathbf{q}+\mathbf{G})\cdot\mathbf{r}} e^{-i(\mathbf{q}+\mathbf{G}')\cdot\mathbf{r}'} \chi_{\mathbf{G}, \mathbf{G}'}(\mathbf{q}, \omega), \quad (2.10)$$

where  $\Omega$  represents the normalization volume, the first sum runs over  $\mathbf{q}$  vectors within the first Brillouin zone (BZ), and  $\mathbf{G}$  and  $\mathbf{G}'$  are reciprocal lattice vectors. Then, introduction of Eq. (2.10) into Eq. (2.6) leads to the following matrix equation:

$$\chi_{\mathbf{G}, \mathbf{G}'}(\mathbf{q}, \omega) = \chi_{\mathbf{G}, \mathbf{G}'}^0(\mathbf{q}, \omega) + \sum_{\mathbf{G}''} \sum_{\mathbf{G}'''} \chi_{\mathbf{G}, \mathbf{G}''}^0(\mathbf{q}, \omega) V_{\mathbf{G}'', \mathbf{G}'''}(\mathbf{q}, \omega) \chi_{\mathbf{G}'', \mathbf{G}'}(\mathbf{q}, \omega), \quad (2.11)$$

where  $V_{\mathbf{G}'', \mathbf{G}'''}(\mathbf{q}, \omega)$  represent Fourier coefficients of the interaction potential of Eq. (2.7). The Fourier coefficients of the density-response function of non-interacting electrons have the well-known form<sup>32</sup>

$$\begin{aligned} \chi_{\mathbf{G}, \mathbf{G}'}^0(\mathbf{q}, \omega) = & \frac{1}{\Omega} \sum_{\mathbf{k}} \sum_{n, n'}^{BZ} \frac{f_{\mathbf{k}, n} - f_{\mathbf{k}+\mathbf{q}, n'}}{E_{\mathbf{k}, n} - E_{\mathbf{k}+\mathbf{q}, n'} + \hbar(\omega + i\eta)} \\ & \times \langle \phi_{\mathbf{k}, n} | e^{-i(\mathbf{q}+\mathbf{G})\cdot\mathbf{r}} | \phi_{\mathbf{k}+\mathbf{q}, n'} \rangle \langle \phi_{\mathbf{k}+\mathbf{q}, n'} | e^{i(\mathbf{q}+\mathbf{G}')\cdot\mathbf{r}} | \phi_{\mathbf{k}, n} \rangle, \end{aligned} \quad (2.12)$$

where the second sum runs over the band structure for each wave vector  $\mathbf{k}$  in the first BZ,  $f_{\mathbf{k}, n}$  are Fermi factors, and  $\phi_{\mathbf{k}, n}(\mathbf{r}, \omega)$  are single-particle Bloch states.

In the RPA, the one-electron Bloch states entering Eq. (2.12) are the self-consistent eigenfunctions of the one-electron Hartree Hamiltonian, and the coefficients  $V_{\mathbf{G}'', \mathbf{G}'''}(\mathbf{q}, \omega)$  entering Eq. (2.11) are the Fourier coefficients of the bare Coulomb interaction. In the

TDLDA, the one-electron Bloch states entering Eq. (2.12) are the self-consistent LDA solutions of the Kohn-Sham equation of DFT, and the coefficients  $V_{\mathbf{G}'',\mathbf{G}'''}(\mathbf{q},\omega)$  entering Eq. (2.11) are the Fourier coefficients of the interaction potential of Eq. (2.7) with the XC kernel of Eq. (2.9).

For the evaluation of the one-electron Bloch states, we first expand them in a plane wave basis,

$$\phi_{\mathbf{k},n}(\mathbf{r}) = \frac{1}{\sqrt{\Omega}} \sum_{\mathbf{G}} u_{\mathbf{k},n}(\mathbf{G}) e^{i(\mathbf{k}+\mathbf{G})\cdot\mathbf{r}}, \quad (2.13)$$

with a kinetic energy cutoff of 12 Rydbergs, which corresponds to keeping approximately 100  $\mathbf{G}$ -vectors in Eq. (2.13). Then we solve for the coefficients  $u_{\mathbf{k},n}$  self-consistently, within a full description of the electron-ion interaction based on the use of a non-local, norm-conserving ionic pseudopotential<sup>33</sup>. We subsequently evaluate, from Eq. (2.12), the Fourier coefficients  $\chi_{\mathbf{G},\mathbf{G}'}^0(\mathbf{q},\omega)$ , which is the most demanding part of the response calculation. Finally, we solve the matrix equation (2.11) for the Fourier coefficients of the interacting response function  $\chi_{\mathbf{G},\mathbf{G}'}(\mathbf{q},\omega)$ , which we obtain in both RPA and TDLDA.

### III. ELECTRONIC STOPPING POWER

We consider a particle of charge  $Z_1$  moving in an inhomogeneous medium. The damping rate of the projectile in the state  $\phi_0(\mathbf{r})$  with energy  $E_0$  is obtained from the knowledge of the imaginary part of the self-energy  $\Sigma(\mathbf{r},\mathbf{r}';E_0)$ , according to:

$$\gamma = -2 \int d\mathbf{r} \int d\mathbf{r}' \phi_0^*(\mathbf{r}) \text{Im}\Sigma(\mathbf{r},\mathbf{r}';E_0) \phi_0(\mathbf{r}'). \quad (3.1)$$

In the so-called GW approximation, the self-energy is given by<sup>27</sup>

$$\Sigma(\mathbf{r},\mathbf{r}';\omega) = \frac{i}{2\pi} \int_{-\infty}^{\infty} d\omega' G(\mathbf{r},\mathbf{r}';\omega - \omega') W(\mathbf{r},\mathbf{r}';\omega'), \quad (3.2)$$

where  $G(\mathbf{r},\mathbf{r}';\omega)$  represents the Green's function for the projectile, and  $W(\mathbf{r},\mathbf{r}';\omega)$  is the screened interaction:

$$W(\mathbf{r}, \mathbf{r}'; \omega) = v(\mathbf{r} - \mathbf{r}') + Z_1^2 \int d\mathbf{r}_1 \int d\mathbf{r}_2 v(\mathbf{r} - \mathbf{r}_1) \chi(\mathbf{r}_1, \mathbf{r}_2, \omega) v(\mathbf{r}_2 - \mathbf{r}'), \quad (3.3)$$

$v(\mathbf{r} - \mathbf{r}')$  being the bare Coulomb interaction and  $\chi(\mathbf{r}, \mathbf{r}', \omega)$  the density-response function of the medium. For periodic crystals, we introduce the Fourier representation given by Eq. (2.10) into Eq. (3.3), and we find that

$$W(\mathbf{r}, \mathbf{r}', \omega) = \frac{Z_1^2}{\Omega} \sum_{\mathbf{q}} \sum_{\mathbf{G}, \mathbf{G}'}^{BZ} e^{i(\mathbf{q} + \mathbf{G}) \cdot \mathbf{r}} e^{-i(\mathbf{q} + \mathbf{G}') \cdot \mathbf{r}'} v_{\mathbf{G}}(\mathbf{q}) [\delta_{\mathbf{G}, \mathbf{G}'} + \chi_{\mathbf{G}, \mathbf{G}'}(\mathbf{q}, \omega) v_{\mathbf{G}'}(\mathbf{q})], \quad (3.4)$$

where  $v_{\mathbf{G}}(\mathbf{q}) = 4\pi/|\mathbf{q} + \mathbf{G}|^2$  are the Fourier coefficients of the bare Coulomb interaction.

Replacing the Green's function entering Eq. (3.2) by its zeroth order approximation, we find the following expression for the damping rate:

$$\gamma = \int_0^\infty d\omega P_\omega, \quad (3.5)$$

where

$$P_\omega = -2 \sum_f \int d\mathbf{r} \int d\mathbf{r}' \phi_f^*(\mathbf{r}') \phi_0^*(\mathbf{r}) \text{Im} W(\mathbf{r}, \mathbf{r}', E_0 - E_f) \phi_f(\mathbf{r}) \phi_0(\mathbf{r}') \delta[\omega - (E_0 - E_f)], \quad (3.6)$$

the sum running over a complete set of final states  $\phi_f(\mathbf{r})$  of energy  $E_f$ .

The quantity  $P_\omega$  entering Eq. (3.5) represents the probability for the projectile to transfer energy  $\omega$  to the medium. Consequently, the stopping power of the medium, i. e., the energy-loss per unit path length of the projectile, can be obtained as follows:

$$-\frac{dE}{dx} = \frac{1}{v} \int_0^\infty d\omega \omega P_\omega, \quad (3.7)$$

where  $P_\omega$  is given by Eq. (3.6).

### A. Random stopping power

In the case of heavy projectiles moving at a constant velocity  $\mathbf{v}$  with no definite impact parameter, the initial and final states can be described by plane waves:

$$\phi_0(\mathbf{r}) = \frac{1}{\sqrt{\Omega}} e^{i\mathbf{q}_0 \cdot \mathbf{r}} \quad (3.8)$$

and

$$\phi_f(\mathbf{r}) = \frac{1}{\sqrt{\Omega}} e^{i(\mathbf{q}_0 - \mathbf{q}) \cdot \mathbf{r}}, \quad (3.9)$$

where  $\mathbf{q}_0$  and  $\mathbf{q}$  represent the initial momentum of the projectile and the momentum transfer, respectively.

For heavy projectiles recoil can be neglected, i.e.,

$$E_0 - E_f = \mathbf{q} \cdot \mathbf{v}, \quad (3.10)$$

and after introduction of Eqs. (3.4), (3.8), (3.9) and (3.10) into Eq. (3.6) we find the following expression for the so-called random stopping power:

$$\left[ -\frac{dE}{dx} \right]_{\text{random}} = -\frac{8\pi}{\Omega v} Z_1^2 \sum_{\mathbf{q}} \sum_{\mathbf{G}} \frac{(\mathbf{q} + \mathbf{G}) \cdot \mathbf{v}}{|\mathbf{q} + \mathbf{G}|^2} \text{Im} \epsilon_{\mathbf{G}, \mathbf{G}}^{-1}[\mathbf{q}, (\mathbf{q} + \mathbf{G}) \cdot \mathbf{v}], \quad (3.11)$$

where  $\epsilon_{\mathbf{G}, \mathbf{G}'}^{-1}(\mathbf{q}, \omega)$  is the inverse dielectric matrix in momentum space:

$$\epsilon_{\mathbf{G}, \mathbf{G}'}^{-1}(\mathbf{q}, \omega) = \delta_{\mathbf{G}, \mathbf{G}'} + \frac{4\pi}{|\mathbf{q} + \mathbf{G}|^2} \chi_{\mathbf{G}, \mathbf{G}'}(\mathbf{q}, \omega), \quad (3.12)$$

the density-response matrix  $\chi_{\mathbf{G}, \mathbf{G}'}(\mathbf{q}, \omega)$  being given by Eq. (2.11).

The symmetry of the one-particle Bloch states results in the following identity:

$$\epsilon_{\mathbf{G}, \mathbf{G}'}^{-1}(S\mathbf{q}, \omega) = \epsilon_{S^{-1}\mathbf{G}, S^{-1}\mathbf{G}'}^{-1}(\mathbf{q}, \omega), \quad (3.13)$$

$S$  representing a point group symmetry operation in the periodic crystal. As a consequence, the stopping power of Eq. (3.11) can be evaluated from the knowledge of the dielectric matrix for wave vectors  $\mathbf{q}$  lying in the irreducible element of the Brillouin zone (IBZ):

$$\left[ -\frac{dE}{dx} \right]_{\text{random}} = -\frac{8\pi}{\Omega v} Z_1^2 \sum_{\mathbf{q}} \sum_S \sum_{\mathbf{G}} \frac{(S\mathbf{q} + \mathbf{G}) \cdot \mathbf{v}}{|S\mathbf{q} + \mathbf{G}|^2} \text{Im} \epsilon_{S^{-1}\mathbf{G}, S^{-1}\mathbf{G}}^{-1}[\mathbf{q}, (S\mathbf{q} + \mathbf{G}) \cdot \mathbf{v}], \quad (3.14)$$

the second sum in this equation running over the symmetry operations generating the wave vectors in the star of each  $\mathbf{q}$ .

If the diagonal elements of the inverse dielectric matrix entering Eq. (3.11) are replaced by the inverse dielectric function of a homogeneous electron gas<sup>5</sup>, i. e.,

$$\epsilon_{\mathbf{G}, \mathbf{G}}^{-1}(\mathbf{q}, \omega) \rightarrow \epsilon_{\text{homog}}^{-1}(|\mathbf{q} + \mathbf{G}|, \omega), \quad (3.15)$$

Eq. (3.11) exactly coincides with the well-known formula for the stopping power of a homogeneous electron gas<sup>34</sup>.



## B. Position-dependent stopping power

In the case of heavy projectiles moving with constant velocity  $\mathbf{v}$  on a definite trajectory at a given impact parameter  $\mathbf{b}$ , the initial and final states can be described in terms of plane waves in the direction of motion and a  $\delta$  function in the transverse direction<sup>35</sup>. Then, introduction of these states,  $\phi_0(\mathbf{r})$  and  $\phi_f(\mathbf{r})$ , and the screened interaction of Eq. (3.4) into Eq. (3.6) gives, after neglecting the projectile recoil, the following result for the position-dependent stopping power:

$$\left[ -\frac{dE}{dx} \right]_{\mathbf{b}} = -\frac{8\pi}{\Omega v} Z_1^2 \sum_{\mathbf{q}}^{\text{IBZ}} \sum_S \sum_{\mathbf{G}} \sum_{\mathbf{K}}' e^{i\mathbf{K} \cdot \mathbf{b}} \frac{(S\mathbf{q} + \mathbf{G}) \cdot \mathbf{v}}{|S\mathbf{q} + \mathbf{G} + \mathbf{K}|^2} \text{Im} \epsilon_{S^{-1}\mathbf{G}, S^{-1}(\mathbf{G} + \mathbf{K})}^{-1} [\mathbf{q}, (S\mathbf{q} + \mathbf{G}) \cdot \mathbf{v}], \quad (3.16)$$

the sum  $\sum_{\mathbf{K}}'$  being restricted to those reciprocal lattice vectors that are perpendicular to the velocity of the projectile, i. e.,  $\mathbf{K} \cdot \mathbf{v} = 0$ .  $\epsilon_{\mathbf{G}, \mathbf{G}'}^{-1}(\mathbf{q}, \omega)$  is the inverse dielectric matrix of Eq. (3.12) and  $S$  represents, as in Eq. (3.14), a symmetry operation of the point group of the periodic crystal.

The most important contribution to the position-dependent stopping power of Eq. (3.16) is provided by the term  $\mathbf{K} = 0$ , the magnitude of the other terms depending on the direction of the velocity. For those directions for which the condition of  $\mathbf{K} \cdot \mathbf{v} = 0$  is never satisfied we have the random stopping power of Eq. (3.14), and for a few highly symmetric or *channeling* directions non-negligible corrections to the random result are found, thus exhibiting the anisotropy of the position-dependent stopping power. We also note that (a) the average over impact parameters of the position-dependent stopping power of Eq. (3.16) along any given channel has the same value as the random stopping power of Eq. (3.14), and (b) as long as the diagonal elements of the so-called dynamical structure factor,  $-2\text{Im}\chi_{\mathbf{G}, \mathbf{G}}(\mathbf{q}, \omega)$ , were isotropic, there would be no dependence of the random stopping power on the direction of  $\mathbf{v}$ .

## IV. RESULTS AND DISCUSSION

The input of our calculation of both random and position-dependent stopping powers of Eqs. (3.14) and (3.16) is the interacting response matrix  $\chi_{\mathbf{G},\mathbf{G}'}(\mathbf{q},\omega)$  of Eq. (2.11), which we have solved for Al crystal. The number of bands required in the evaluation of the polarizability  $\chi_{\mathbf{G},\mathbf{G}'}^0(\mathbf{q},\omega)$  of Eq. (2.12) depends on the value of the frequency  $\omega$ . As the maximum energy  $\omega$  transferred by the moving projectile to the target is proportional to the velocity, only a few bands are required in the case of slow projectiles. Indeed, it has been found<sup>22</sup> that at velocities below  $v = 0.1\text{a.u.}$  just two bands are required to account for the energy-loss. At larger velocities excitations to higher bands become possible, and we find that convergence is achieved, for  $v < 2\text{a.u.}$ , if one considers on the order of 30 bands. The results presented below have been found to be well-converged for all velocities under study, and they all have been performed with the use of 60 bands.

The sampling of the BZ required for the evaluation of both the polarizability of Eq. (2.12) and the stopping powers of Eqs. (3.14) and (3.16) has been performed on  $10 \times 10 \times 10$  Monkhorst-Pack meshes<sup>36</sup> (47 points in the IBZ) with an energy smearing of the Fermi level of 0.25eV, and this sampling has been done in conjunction with a choice of a finite value of the damping factor entering Eq. (2.12) of  $\eta = 1.5\text{eV}$ . At velocities of the projectile below the velocity for which plasmon excitation becomes possible, convergence is already achieved with the use of  $4 \times 4 \times 4$  Monkhorst-Pack meshes (8 points in the IBZ).

### A. Random stopping power

The main ingredient in the calculation of the random stopping power of Eq. (3.14) is the so-called dynamical structure factor  $S_{\mathbf{G}}(\mathbf{q},\omega)$ . It is proportional to the diagonal elements of the imaginary part of the density-response matrix:

$$S(\mathbf{q} + \mathbf{G}, \omega) = -2\text{Im}\chi_{\mathbf{G},\mathbf{G}}(\mathbf{q}, \omega)$$

$$= -\frac{|\mathbf{q} + \mathbf{G}|^2}{2\pi} \text{Im}\epsilon_{\mathbf{G},\mathbf{G}}^{-1}(\mathbf{q}, \omega), \quad (4.1)$$

where  $\mathbf{q}$  is taken to be in the first BZ. Thus, couplings of the wave vector  $\mathbf{q} + \mathbf{G}$  to wave vectors  $\mathbf{q} + \mathbf{G}'$  with  $\mathbf{G} \neq \mathbf{G}'$ , which appear as a consequence of the existence of electron density variations in real solids, only contribute to the random stopping power through the dependence of the diagonal elements of the interacting response matrix  $\chi_{\mathbf{G},\mathbf{G}}(\mathbf{q}, \omega)$  on the off-diagonal elements of the polarizability  $\chi_{\mathbf{G},\mathbf{G}'}^0(\mathbf{q}, \omega)$ . We have found that in the case of Al crystal, which does not present strong electron density gradients nor special electron density directions (bondings), contributions from these so-called crystalline local field effects are within 0.5% of the total random stopping power. Thus, as for the evaluation of the random stopping power of Al crystal, the off-diagonal elements of  $\chi_{\mathbf{G},\mathbf{G}'}^0(\mathbf{q}, \omega)$  can be neglected.

In the general case of an inhomogeneous system one finds, for the imaginary part of the inverse dielectric function, the following form of the f-sum-rule:

$$\int_0^\infty d\omega \omega \text{Im}\epsilon_{\mathbf{G},\mathbf{G}'}^{-1}(\mathbf{q}, \omega) = -2\pi^2 n_{\mathbf{G}-\mathbf{G}'}, \quad (4.2)$$

where  $n_{\mathbf{G}}$  represent the Fourier components of the density. Note that  $n_{\mathbf{G}=0}$ , which equals the average density of the system, does not depend on the details of the band structure. Thus, it may be argued that band structure effects, which have an impact on both plasmon dispersion<sup>7</sup> and the dynamical structure factor<sup>10</sup>, may give no corrections to integrated quantities as the random stopping power. However, because in the sum over the wave vector  $\mathbf{q}$  in Eq. (3.14) the frequency  $\omega$  in the argument of the structure factor takes values from 0 to only  $|\mathbf{q} + \mathbf{G}|v$ , the stopping power of band electrons and that of electrons in an effective jellium with the same average electron density will be, in general, different.

In Fig. 1 we show, as a function of the velocity of the projectile, our full calculation of the random stopping power (see Eq. (3.14)) of valence electrons in Al crystal for protons ( $Z_1 = 1$ ), together with the corresponding result for a homogeneous electron gas with an electron density parameter equal to that of aluminum ( $r_s = 2.07$ )<sup>37</sup>. In the calculation of the stopping power of both band and jellium electrons, the third sum in Eq. (3.14) is extended over  $15\mathbf{G}$

vectors of the reciprocal lattice, the magnitude of the maximum momentum transfer  $\mathbf{q} + \mathbf{G}$  being  $2.9q_F$  ( $q_F$  is the Fermi momentum)<sup>38,39</sup>. Solid and open circles represent our calculated random stopping powers of band electrons, as calculated within the RPA and the TDLDA, respectively. Solid and dashed lines represent the corresponding stopping powers of jellium electrons. All these results have been found, for Al crystal, to be insensitive to the choice of the projectile velocity direction.

In the case of projectiles moving at low velocities, below the threshold velocity for plasmon excitation, the sum over the frequency  $\omega = (\mathbf{q} + \mathbf{G}) \cdot \mathbf{v}$  in Eq. (3.14) can never be replaced by an integration from 0 to  $\infty$  as in Eq. (4.2), and the stopping power will, in principle, depend on the band structure of the crystal. The existence of interband transitions, not present within a jellium model of the crystal, result in a dynamical structure factor which is, at low frequencies (where it increases linearly with frequency), slightly enhanced with respect to the corresponding jellium result<sup>10</sup>. As a result, the stopping power of the real target is, for projectile velocities smaller than the Fermi velocity and within both RPA and TDLDA, a linear function of the velocity and about 7% higher than the stopping power of jellium electrons.

The threshold velocity for which plasmon excitation becomes possible is  $v_t \approx 1.3\text{a.u.}$  in the case of electrons in jellium with  $r_s = 2.07$ . In the case of Al crystal this threshold velocity is slightly smaller ( $v \approx 1.2\text{a.u.}$ ), as can be easily concluded from an inspection of the plasmon dispersion curve for Al crystal of Ref. 7. For projectile velocities larger than  $v_t$  there are two mechanisms of valence electron excitation: (a) excitation of single electron-hole pairs and (b) excitation of plasmons. Figure 2 exhibits, as a function of the projectile velocity, separate contributions to the stopping power of both band (solid circles) and jellium (solid lines) electrons coming from electron-hole pair excitation (Fig. 2a) and plasmon excitation (Fig. 2b). Although for wave vectors that are smaller than  $q_c$  (the critical wave vector where the plasmon dispersion enters the electron-hole pair excitation spectrum) both mechanisms of valence electron excitation contribute to the energy-loss, contributions from losses to electron-hole pair excitations are negligible for  $q < q_c$ , and Eq. (4.2) leads

us to the conclusion that contributions from losses to plasmon excitation are independent of the detailed band structure of the crystal. That this is the case is obvious from Fig. 2b. As for the contribution to the energy-loss coming from the excitation of electron-hole pairs, Figs. 1 and 2a show that band structure corrections lower the stopping power of electrons in jellium by about 10% at and just above the plasmon threshold velocity; this is a consequence of the dynamical structure factor for the real crystal being, within the electron-hole pairs continuum at  $q > q_c$  and  $\omega < (q + G)v$ , smaller than in the case of a homogeneous electron gas. Nevertheless, contributions to the stopping power coming from the excitation of plasmons are still smaller than contributions from losses to electron-hole pairs, and there is, at high velocities, exact equipartition of the energy-loss, as in the case of a homogeneous electron gas<sup>40</sup>. Also, at high velocities the sum over the frequency  $\omega = (\mathbf{q} + \mathbf{G}) \cdot \mathbf{v}$  in Eq. (3.14) can be replaced by an integration from 0 to  $\infty$  and the stopping power of both jellium and band electrons is expected to be the same, as illustrated in Figs. 1 and 2a.

We note that the TDLDA results plotted in Fig. 1 for the stopping power of jellium electrons, which describe short-range correlation effects within the LDA, approximately reproduce more detailed calculations with either static or dynamic local-field corrections included<sup>41</sup>. The stopping power of both jellium and band electrons is enhanced by about 20%, at low velocities (exclusive electron-hole pairs domain), with respect to the RPA result, as a consequence of short-range correlation effects provoking a reduction in the screening within the target. The sum rule of Eq. (4.2) equally applies for both RPA and TDLDA dynamical structure factors, and this prevents, therefore, plasmon contributions to the stopping power from being sensitive to the details of the wave-vector and frequency dependence of the response. At large velocities, well above the stopping maximum, all calculations presented in Fig. 1 converge to the well-known Bethe formula<sup>34</sup>, in which the mean excitation potential is replaced by the plasma energy<sup>42</sup>.

## B. Position-dependent stopping power

We have carried out, from Eq. (3.16), calculations of the electronic energy-loss versus impact parameter, and we have obtained, within the RPA, the results presented in Fig. 3. In this figure we represent by solid curves the position-dependent stopping power of Al crystal for protons ( $Z_1 = 1$ ) moving with  $v = 0.2a.u.$  along the (100) (Fig. 3a) and (111) (Fig. 3b) directions. In Fig. 3a the impact parameter has been taken to be  $\mathbf{b} = (0, b, 0)a_c$  ( $a_c$  is the lattice constant), with  $b$  from 0 to 1, and in Fig. 3b it has been taken to be  $\mathbf{b} = (-1 \ 1 \ 0)a_c$ . Contour density plots of the square lattice containing both the projectile trajectory and the  $\mathbf{b}$  vector are displayed in Figs. 4a and 4b for the (100) and (111) directions, respectively. The averaged electronic densities along the projectile paths depicted in Fig. 4 are plotted in Fig. 5, as a function of the impact parameter, showing for this fcc crystal the expected periodicity with  $b = 1/2$ , also present in the position-dependent stopping power of Fig 3.

First of all, we note that the existence of small electron density variations in real aluminum results, through the off-diagonal elements of the interacting density-response function  $\chi_{\mathbf{G},\mathbf{G}'}(\mathbf{q},\omega)$ , in non-negligible differences between position-dependent and random stopping powers. We have obtained differences up to 20% for projectiles incident in the (100) direction (see Fig. 3a), and up to 10% for projectiles moving in the (111) direction (see Fig. 3b). The maxima in the stopping power for trajectories along the interstitial regions ( $b = 1/4$ ) and the minima near the cores ( $b=0$ ) are associated with corresponding maxima and minima in the integrated electronic densities of Fig. 5.

A comparison with a local density approximation (LDA)<sup>43</sup> is also shown in Fig. 3 (dashed curves). In this approach, the position-dependent stopping power is obtained as the stopping power of a homogeneous electron gas with an electron density equal to the average electron density along the projectile path. Although the impact parameter dependence, as obtained in this approach, is qualitatively the same as found within our full band structure calculation, position-dependent corrections to the random stopping power appear to be largely underestimated within the LDA. This is obviously a consequence of the stopping power

depending not only on the local density, but also on the electron density gradients further away from the projectile trajectory. We have also calculated position-dependent stopping powers of Al crystal for various non-relativistic velocities of the incident projectile, and we have found that corrections to the random stopping power, as obtained within the LDA, are too small for all velocities. These corrections are found, within our full treatment of the band structure, to slightly decrease with the velocity of the projectile. In the case projectiles moving near the cores ( $b = 0$ ) along the (100) direction, we have obtained differences between position-dependent and random stopping powers of approximately 20% – 12% in the velocity range from  $v = 0.2$  a.u. to  $v = 1$  a.u.. For projectiles moving near the cores ( $b = 0$ ) along the (111) direction, these differences have been found to be, in the same velocity range, of approximately 10% – 8%.

## V. CONCLUSIONS

We have presented full band structure calculations of both random and position-dependent stopping powers of valence electrons in Al crystal, as obtained within linear-response theory and with the use of the RPA and the TDLDA. The random stopping power has been evaluated for a wide range of projectile velocities. Our results indicate that at low velocities of the projectile band structure effects result in the stopping power of real aluminum being about 7% higher than that of a homogeneous electron gas with a density equal to the average electron density of the real crystal ( $r_s = 2.07$ ). At velocities just above the threshold velocity for plasmon excitation, the stopping power of valence electrons in Al crystal is found to be smaller than that of jellium electrons, corrections being of about 10%. In the high-velocity limit, the stopping power of both jellium and band electrons is found to be the same and to coincide with the well-known Bethe formula.

The various contributions to the random stopping power of Al crystal have been calculated separately, showing that band structure effects on the contribution to the stopping power coming from plasmon excitation are negligible. This result has been shown to be a

consequence of the dynamical structure factor of both jellium and real aluminum fulfilling the same sum rule, as long as the average electron density is the same. Also, there is, in the high-velocity limit, exact equipartition for the energy-loss, as in the case of a homogeneous electron gas.

The position-dependent stopping power has been evaluated for projectiles with velocities up to the Fermi velocity incident in various high-symmetry directions. We have found differences between position-dependent and random stopping powers up to 10% for projectiles incident in the (100) direction and up to 20% for projectiles moving in the (111) direction. The magnitude of these position-dependent relative corrections to the random stopping power has been found to be, within the LDA, largely underestimated, specially at high velocities of the projectile.

#### ACKNOWLEDGMENTS

We thank Alberto García for his help in the calculation of the one-electron Bloch states. I.C. and J.M.P. acknowledge partial support by the Basque Unibertsitate eta Ikerketa Saila and the Spanish Ministerio de Educación y Cultura. A.G. Eguiluz acknowledges support from National Science Foundation Grant No. DMR-9634502 and from the National Energy Research Supercomputer Center. ORNL is managed by Lockheed Martin Energy Research Corp. for the U.S. DOE under contract No. DE-AC05-96OR22464.



## REFERENCES

- <sup>1</sup> N. Bohr, Philos. Mag. **25**, 10 (1913); **30**, 581 (1915).
- <sup>2</sup> H. Bethe, Ann. Phys. (Leipzig) **5**, 325 (1930).
- <sup>3</sup> F. Bloch, Ann. Phys. (Leipzig) **16**, 285 (1933); Z. Phys. **81**, 363 (1933).
- <sup>4</sup> E. Fermi and E. Teller, Phys. Rev. **72**, 399 (1947).
- <sup>5</sup> J. Lindhard, K. Dan. Vidensk. Selsk. Mat. Fys. Medd. **28** (8), 1 (1954).
- <sup>6</sup> R. H. Ritchie, Phys. Rev. **114**, 644 (1959).
- <sup>7</sup> A. A. Quong and A. G. Eguiluz, Phys. Rev Lett. **70**, 3955 (1993); A. Fleszar, R. Stumpf, and A. G. Eguiluz, Phys. Rev. B **55**, 2068 (1997).
- <sup>8</sup> F. Aryasetiawan and K. Karlsson, Phys. Rev. Lett. **73**, 1679 (1994).
- <sup>9</sup> N. E. Maddocks, R. W. Godby, and R. J. Needs, Europhys. Lett. **27**, 681 (1994); Phys. Rev. B **49**, 8502 (1994).
- <sup>10</sup> A. Fleszar, A. A. Quong, and A. G. Eguiluz, Phys. Rev. Lett. **74**, 590 (1995).
- <sup>11</sup> P. L. Grande and G. Schiwietz, Phys. Lett. A **163**, 439 (1992).
- <sup>12</sup> J. J. Dorado and F. Flores, Phys. Rev. A **47**, 3062 (1993).
- <sup>13</sup> S. L. Adler, Phys. Rev. **126**, 413 (1962).
- <sup>14</sup> N. Wiser, Phys. Rev. **129**, 62 (1963).
- <sup>15</sup> W. M. Saslow and G. F. Reiter, Phys. Rev. B **7**, 2995 (1973).
- <sup>16</sup> F. F. Komarov and M. A. Kumakhov, Rad. Effects **22**, 1 (1974).
- <sup>17</sup> A. Desalvo and R. Rosa, J. Phys. C **10**, 1595 (1977).
- <sup>18</sup> H. Esbensen and J. A. Golovchenko, Nucl. Phys. A **298**, 382 (1978).

- <sup>19</sup> A. F. Burenkov, F. F. Komarov and M. A. Kumakhov, Phys. Status Solidi B **99**, 417 (1980).
- <sup>20</sup> O. H. Crawford and C. W. Nestor, Phys. Rev. A **28**, 1260 (1983).
- <sup>21</sup> T. M. H. E. Tielens, Gerrit E. W. Bauer and T. H. Stoof, Phys. Rev. B **49**, 5741 (1994).
- <sup>22</sup> J. M. Pitarke, I. Campillo, and A. G. Eguiluz, in *Proceedings of the 17th Werner Brandt Workshop on Charged Particle Penetration Phenomena*, Charlottesville, Virginia, 1997.
- <sup>23</sup> R. J. Mathar, S. B. Trickey, and J. R. Sabin, in *Proceedings of the 17th Werner Brandt Workshop on Charged Particle Penetration Phenomena*, Charlottesville, Virginia, 1997.
- <sup>24</sup> I. Campillo, J. M. Pitarke, A. G. Eguiluz and Alberto Garcia, Nucl. Instr. and Meth. B **135**, 103 (1998).
- <sup>25</sup> See, e.g., D. Pines, Elementary excitations in solids, Chapter 3 (Addison Wesley, New York, 1963).
- <sup>26</sup> A. Zangwill and P. Soven, Phys. Rev. A **21**, 1561 (1980).
- <sup>27</sup> L. Hedin and S. Lundqvist, in *Solid State Physics: Advances in Research and Applications*, edited by E. H. Ehrenreich and D. Turnbull (Academic, New York, 1969), Vol. 23, p. 1.
- <sup>28</sup> E. K. U. Gross, J. F. Dobson and M. Petersilka, in *Density Functional Theory II*, edited by R. F. Nalewajski, "Topics in Current Chemistry", Vol. 181 (Springer, Berlin, 1996).
- <sup>29</sup> E. Runge and E. K. U. Gross, Phys. Rev. Lett. **52**, 997 (1984).
- <sup>30</sup> P. Hohenberg and W. Kohn, Phys. Rev. **136**, B864 (1964); W. Kohn and L. Sham, Phys. Rev. **140**, A1133 (1965).
- <sup>31</sup> D. M. Ceperley and B. J. Alder, Phys. Rev. Lett. **45**, 566 (1980); J. Perdew and A. Zunger, Phys. Rev. B **23**, 5048 (1981).
- <sup>32</sup> A. G. Eguiluz, A. Fleszar, and J. A. Gaspar, Nucl. Instrum. Methods B **96**, 550 (1995).

- <sup>33</sup> D. R. Hamann, M. Schluter, and C. Chiang, Phys. Rev. Lett. **43**, 1494 (1979); D. R. Hamann, Phys. Rev. B **40**, 2980 (1989).
- <sup>34</sup> P. M. Echenique, F. Flores, and R. H. Ritchie, in *Solid State Physics: Advances in Research and Applications*, edited by E. H. Ehrenreich and D. Turnbull (Academic, New York, 1990), Vol. 43, p. 229.
- <sup>35</sup> P. M. Echenique, J. Bausells, and A. Rivacoba, Phys. Rev. B **35**, 1521 (1987); R. H. Ritchie and A. Howie, Phil. Mag. A **58**, 753 (1988); J. M. Pitarke and A. Rivacoba, Surf. Sci. **377**, 294 (1997).
- <sup>36</sup> H.J. Monkhorst and J.D. Pack, Phys. Rev. B **13**, 5188 (1976).
- <sup>37</sup> The electron density parameter,  $r_s$ , represents the average interelectronic distance, i. e.,  $n_0^{-1} = (4\pi/3)/r_s^3$ ,  $n_0$  being the average electron density.
- <sup>38</sup> If more than 15 $\mathbf{G}$  vectors had been taken in the calculation of Eq. (3.14), more than 60 bands would have been required for the the stopping power with projectile velocities up to  $v = 4\text{a.u.}$  to be well-converged.
- <sup>39</sup> Contributions to the stopping power of a homogeneous electron gas are well-known to come, within the RPA, from all wave vectors which are smaller than  $2(q_F + v)$ , and our calculated results of Fig. 1 are, therefore, expected to underestimate the total stopping power of both jellium and band electrons for all velocities  $v > 0.5\text{a.u.}$ . However, we have found that differences, at large wave vectors, between the integrated dynamical structure factor for jellium and band electrons are very small, and the results of Fig. 1 provide, therefore, an accurate measure of the effect of the band structure on the random stopping power of valence electrons.
- <sup>40</sup> J. Lindhard, A. Winther and K. Dan, Vidensk. Selsk. Mat.-Fys. Medd. **34**(4), 1-22 (1964).
- <sup>41</sup> See, e.g., N-P. Wang and I. Nagy, Phys. Rev. A **55**, 2083 (1997), and references therein.

<sup>42</sup> The Bethe formula is, in the high velocity limit, nearly insensitive to differences among the plasma frequencies obtained in the various approximations to the response of the target.

<sup>43</sup> The use of this so-called local density approximation (LDA) should not be confused with the use, within DFT, of the LDA for the evaluation of  $V_{xc}$  and the kernel  $K_{xc}$  of Eqs. (2.5) and (2.8).

## FIGURES

FIG. 1. Full band structure calculation, from Eq. (3.14), of the random stopping power of valence electrons in Al crystal for protons ( $Z_1 = 1$ ), as a function of the projectile velocity. Solid and open circles represent the results obtained in the RPA and the TDLDA, respectively. RPA and TDLDA stopping powers of electrons in an homogeneous electron gas with  $r_s = 2.07$  are represented by solid and dashed lines, respectively.

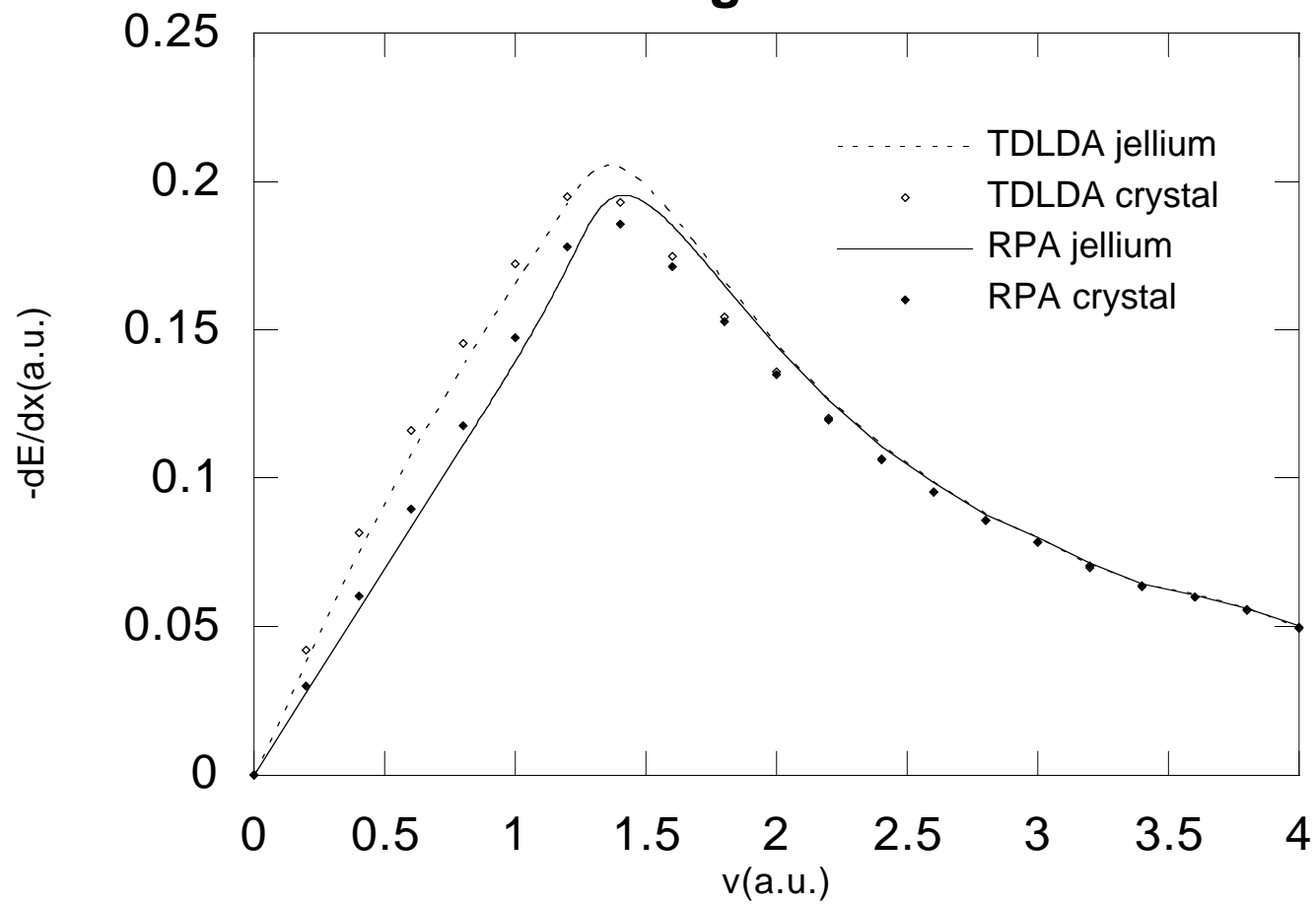
FIG. 2. Contributions to the random stopping power of valence electrons in Al crystal coming from the excitation of (a) electron-hole pairs and (b) plasmons, versus the projectile velocity, as obtained from Eq. (3.14) within the RPA. Full band structure calculations are represented by solid circles. The corresponding jellium results are represented by solid lines.

FIG. 3. Position-dependent stopping power of Al crystal for protons moving with  $v = 0.2$ , as obtained within the RPA. The projectile is incident in the (1 nm) direction and the stopping power is plotted as a function of the magnitude of the impact vector along the  $(\alpha \beta \gamma)$  direction, with (a) (1 nm)=(100) and  $(\alpha \beta \gamma)=(010)$ ; (b) (1 nm)=(111) and  $(\alpha \beta \gamma)=(-1 1 0)$ . Solid lines represent full band structure calculations, as obtained from Eq. (3.16). Dashed curves represent LDA calculations, obtained as explained in the text, and the horizontal dashed line represents the stopping power of a homogeneous electron gas with  $r_s = 2.07$ . All results have been normalized to the value of the random stopping power of Al crystal for the same velocity.

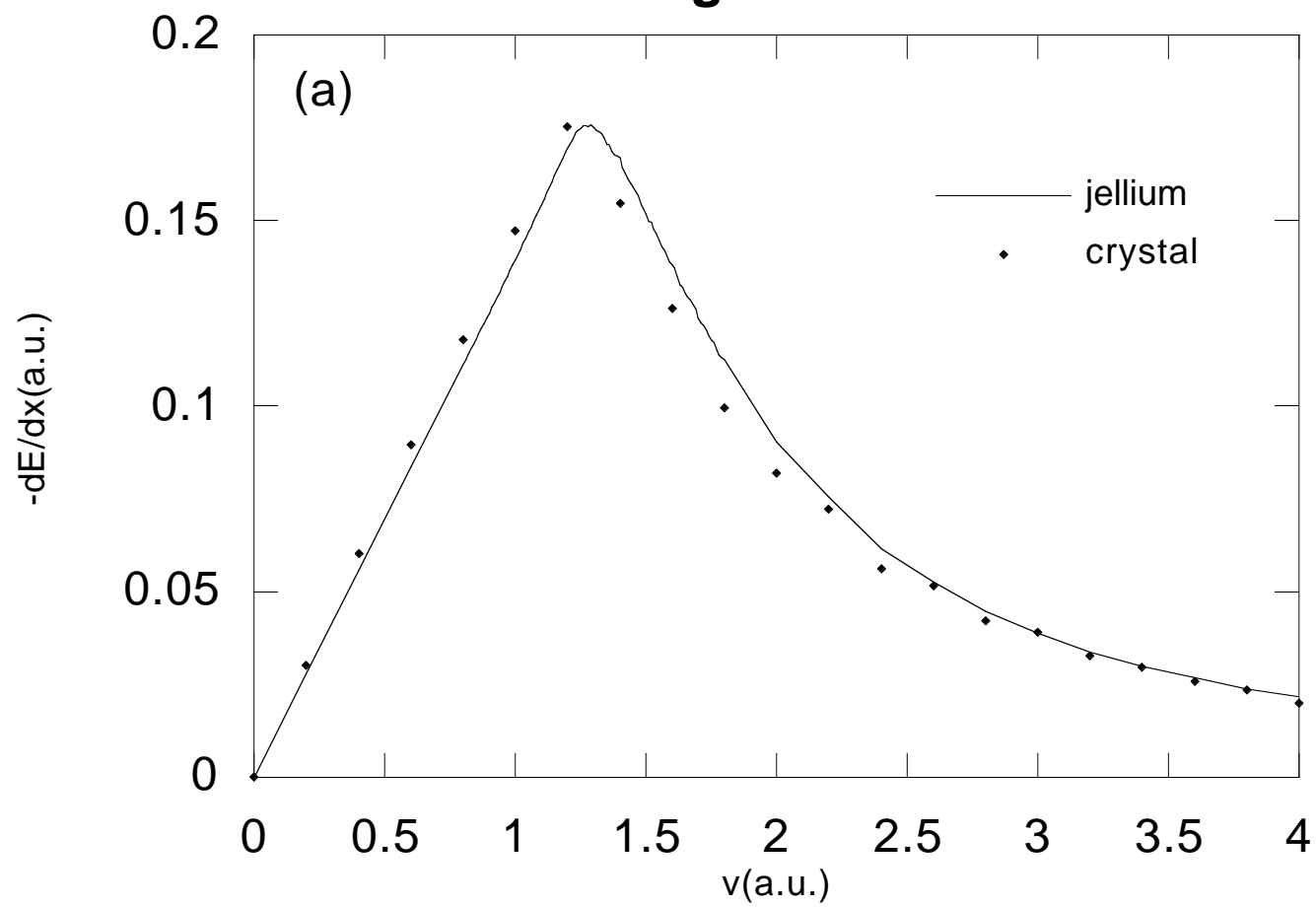
FIG. 4. Contour valence-density plots of the square lattice containing the projectile trajectory (1 nm) and the impact vector  $(\alpha \beta \gamma)$ , with: (a) (1 nm)=(100) and  $(\alpha \beta \gamma)=(010)$ ; (b) (1 nm)=(111) and  $(\alpha \beta \gamma)=(-1 1 0)$ . Projectile trajectories with  $b = 1/4$  are also represented.

FIG. 5. Averaged valence-densities along the projectile paths depicted in Fig. 4, as a function of the impact parameter  $b$ . The solid line corresponds to a projectile trajectory along the (100) direction, as in Figs. 3a and 4a. The dashed line corresponds to a projectile trajectory along the (111) direction, as in Figs. 3b and 4b. All results have been normalized to the value of the average valence-density of Al,  $n_0$ .

**Figure 1**



**Figure 2a**



**Figure 2b**

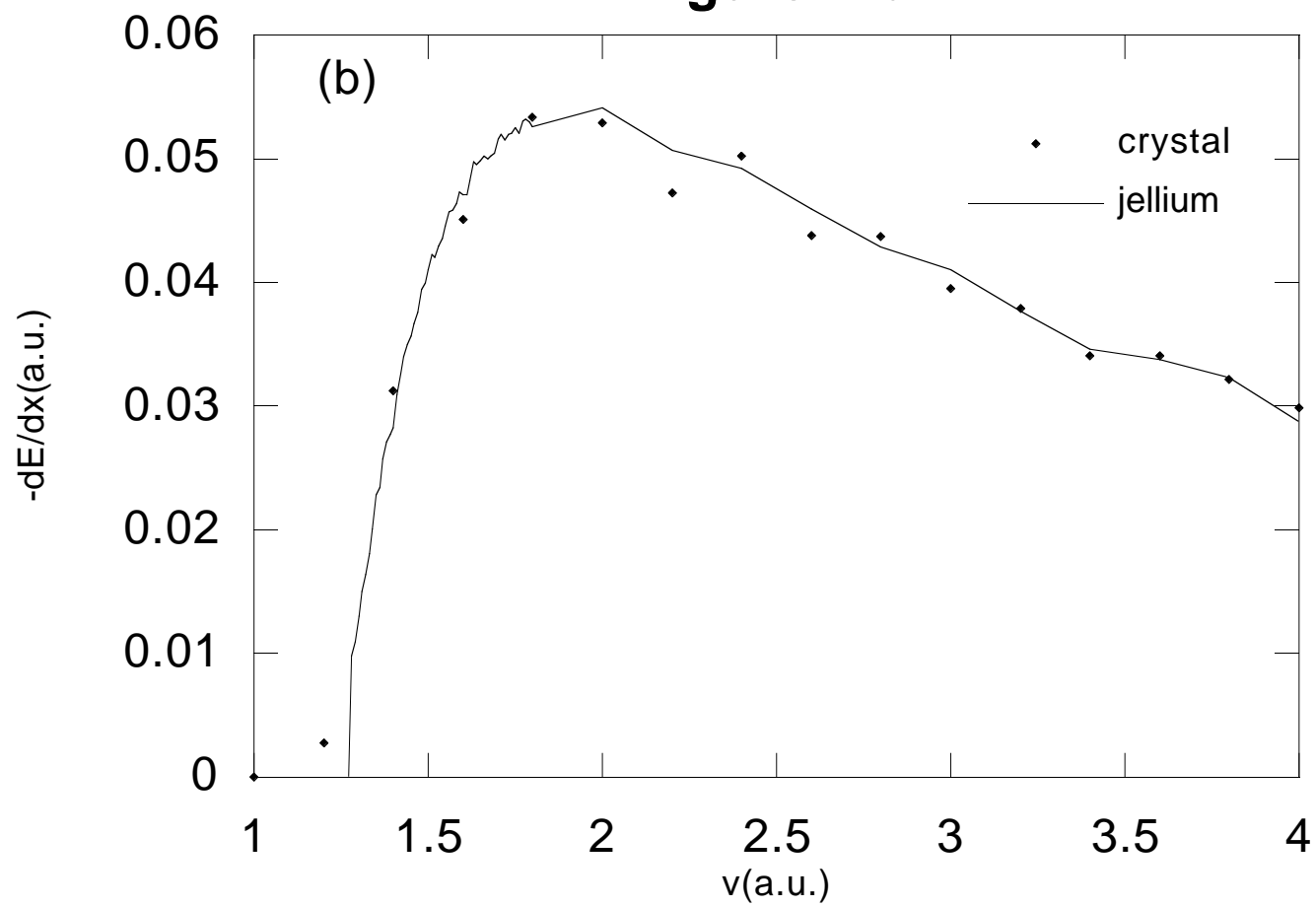




**figure 3a**

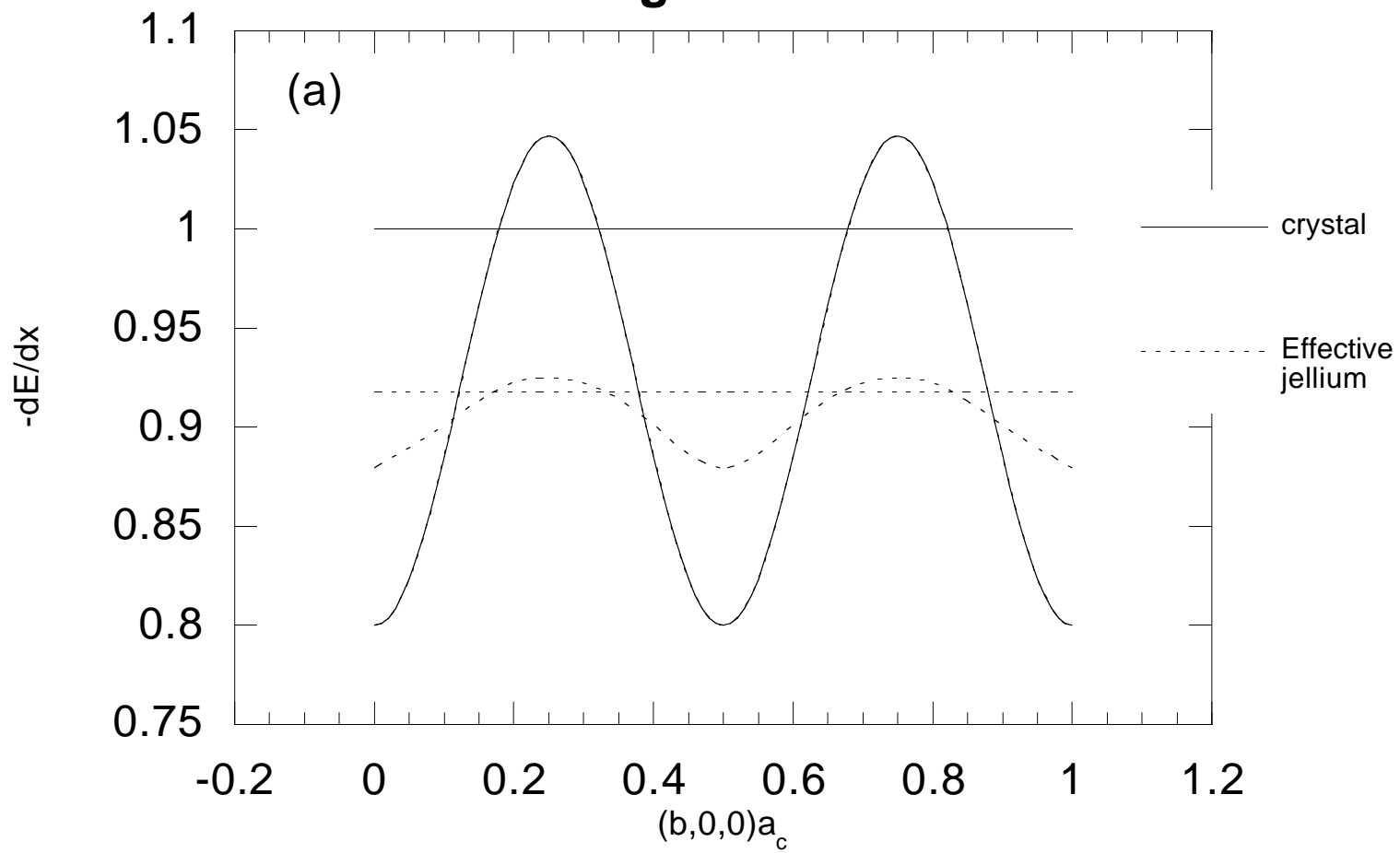


**figure 3b**

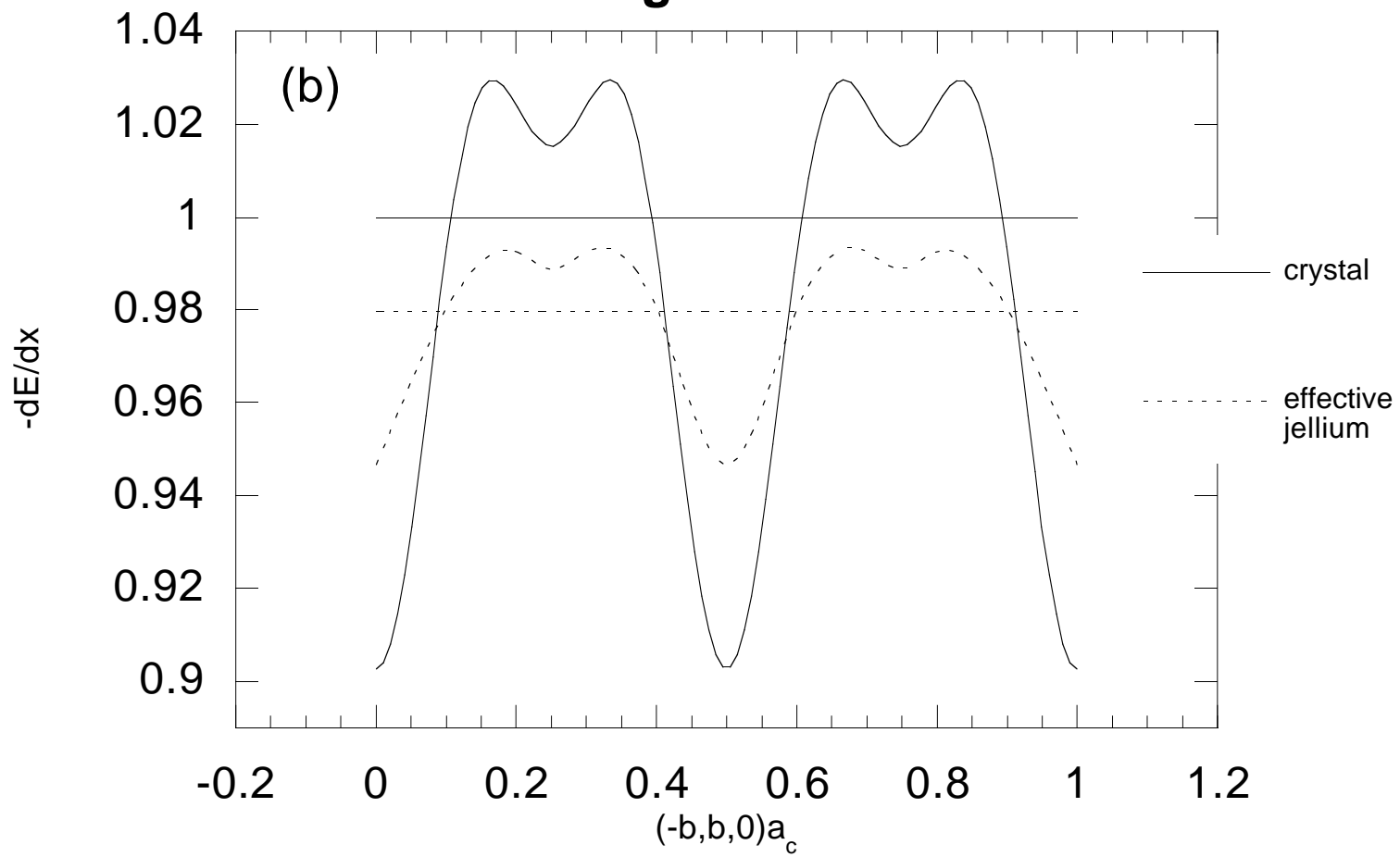


figure4a

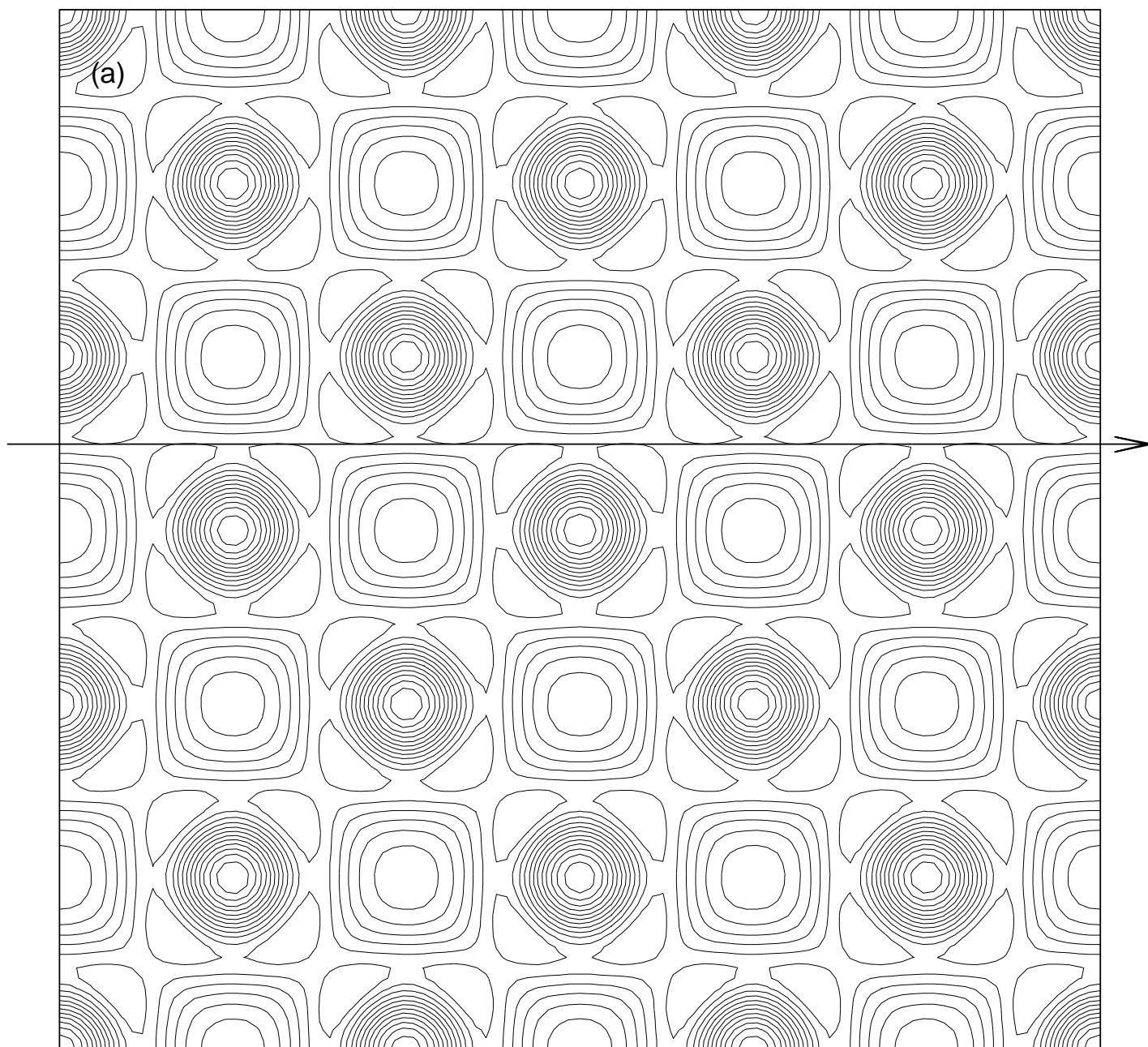
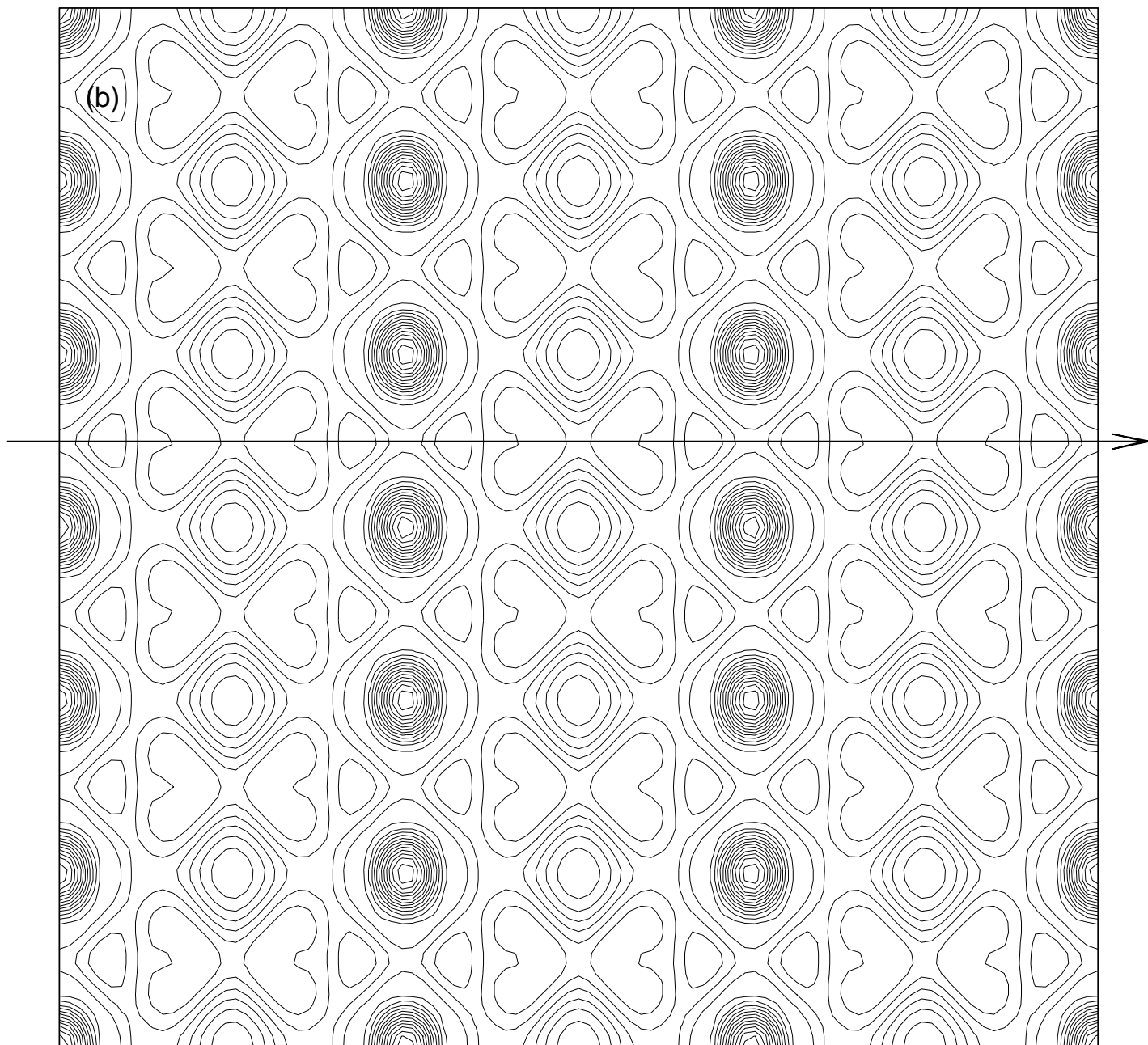


figure 4b



**Figure 5**

